ChemComm
Chemical Communications

Accepted Manuscript

This article can be cited before page numbers have been issued, to do this please use: L. Zhao, X. Kuang, C. Chen, X. Sun, Z. Wang and Q. Wei, *Chem. Commun.*, 2019, DOI: 10.1039/C9CC04378K.

ROYAL SOCIETY OF CHEMISTRY

rsc.li/chemcomm

ROYAL SOCIETY OF CHEMISTRY View Article Online
DOI: 10.1039/C9CC04378K

Journal Name

COMMUNICATION

Boosting Electrocatalytic Nitrogen Fixation Via Energy-Efficient Anodic Oxidation of Sodium Gluconate

Received 00th January 20xx,
Accepted 00th January 20xx

DOI: 10.1039/x0xx00000x

www.rsc.org/

Lu Zhao, Xuan Kuang*, Cheng Chen, Xu Sun, Zhiling Wang, and Qin Wei*

Here, we report an anodic replacement of the water oxidation reaction with more readily oxidizable species to facilitate ambient electrocatalytic nitrogen reduction reaction (NRR). A self-supported catalyst, Cu^{II}-MOF on carbon cloth (JUC-1000/CC) act as versatile cathode and anode for both NRR and electro-oxidation of sodium gluconate (ECSG) to glucaric acid (GA). Impressively, the two-electrode system requires a potential of only 0.4 V to achieve NH_3 yield rate of 24.7 mg h^{-1} mg cat^{-1}, FE of 11.90% and SA selectivity of 96.96%, and behaves strong electrochemical stability. This study reveals that the strategy avoids sacrificing the NH_3 yield to increase FE, and offers an efficient electrosynthesis of NH_3 and SA simultaneously.

Industrially, artificial N_2 fixation to NH_3 is still dominated by traditional Haber-Bosch process under severe conditions, and consumes large amount of high-purity H_2 and 1-2% of the world's annual energy supply.[1-3] Electrocatalytic N_2 reduction reaction (NRR) is a promising alternative since it can allow NH_3 production under ambient conditions directly from N_2 and H_2O powered by renewable electricity.[4,5] However, the NRR process requires high overpotential to break the high triple-bond energy of N≡N (941 kJ·mol^{-1}) and is severely hindered by competing hydrogen evolution reaction (HER), which result in a Faradaic efficiency (FE) of less than 10% or even less than 1% and low NH_3 yield rate.[6]

Electrolytes are considered as a major part of electrochemical NRR systems. To circumvent HER and improve selectivity, a few innovative electrolytes including proton exchange electrolyte, anion exchange electrolyte have been investigated by restricting the electron and proton transfer rate and increasing solubility of N_2.[7-9] However, these efforts come at the expense of system efficiency and high cost of electrolyte additives other than water, which make it a barrier for industrial-scale application. It is known that electrochemical NRR systems are consist of two half-reactions, N_2 reduction at the cathode and water oxidation at the anode. The water oxidation also requires high overpotential, and its product, O_2, is not of high value to the process. Hence, an attractive energy-saving strategy is to replace water oxidation by thermodynamically more favorable oxidation reactions into high value-added products at the anode and provide electrons to the cathode side for NRR. Predictably, such design may improve the NH_3 yield while simultaneously maintaining high FE even though accompanied with hydrogen evolution, which, however, has not been reported to date.

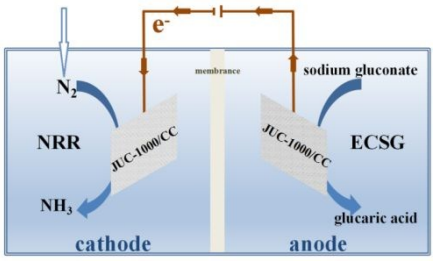

Fig. 1 Illustration of electrocatalytic conversion of sodium gluconate into glucaric acid integrated with NH_3 production in H-type electrolytic cell device.

As a proof of concept, herein, we report a integrated catalytic system, coupling selective electro-oxidation of sodium gluconate (ECSG) to glucaric acid (GA) and NRR (Fig. 1). GA is a high-value-added chemical due to its crucial role in food additives, nylons and plastics industries.[10] And it is also an essential precursor for the product of adipic acid as one of the most widely used non-food biomass materials in the industry for minimizing dependence on petroleum.[11-13] The catalytic oxidation of sodium gluconate (SG) to GA by electrochemistry can faultlessly avoid the generation of significant amounts of toxic by-products and inorganic salts from commonly used chemical oxidation of glucose.[10] Considering the benefits of the high specific surface area and porosity, we prepared a self-supported Cu^{II}-MOF (JUC-1000)[14] on carbon cloths (denoted as JUC-1000/CC) as the catalyst. Encouragingly, when

[a] School of Chemistry and Chemical Engineering, University of Jinan, Jinan 250022, P. R. China.
[b] Key Laboratory of Interfacial Reaction & Sensing Analysis in Universities off Shandong, Shandong Provincial Key Laboratory of Fluorine Chemistry and Chemical Materials, Jinan 250022, P. R. China
E-mail: chm_weiq@ujn.edu.cn, chm_kuangx@ujn.edu.cn
† Electronic supplementary information (ESI) available: Full synthetic and experimental details, additional figures and images. See DOI:

utilized as catalysts for both cathode and anode, the assembled electrolyzer achieves a FE as high as 11.9% with a NH_3 yield of 24.7 mg h^{-1} mg_{cat}^{-1}, and GA selectivity of 96.96% at 0.4 V (vs. RHE). Moreover, it shows strong catalytic stability.

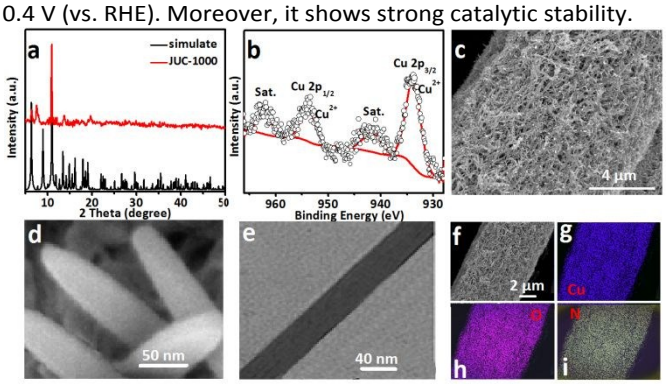

Fig. 2 (a) XRD patterns of as-prepared and simulated JUC-1000. (b) XPS spectra in Cu 2p regions for JUC-1000. (c, d and f) Low- and high-magnification SEM images, (e) TEM image of JUC-1000. (g-i) EDX elemental mapping images of Cu, N and O for JUC-1000/CC.

Typically, the JUC-1000/CC electrocatalyst was prepared by a convenient electrodeposition method in a mixed solution of DMF and water at -1.5 V for 15 min at room temperature. As shown from the crystal structure (Fig. S1, ESI), Cu atoms in JUC-1000 are rare 5-coordinate modes from four carboxylate groups and with either a N atom in the L ligand or a water molecule, forming three types of polyhedron with three types of pores (7.3, 10.9 and 13.6 Å),[14] which covalently bonded into the 3D network $[Cu_{24}L_{12}(H_2O)_{12}]\cdot 30DMF\cdot 14H_2O$. The open metal sites and further dehydration will enhance its catalytic activity. Fig. 2a shows X-ray powder diffraction (XRD) patterns of as-synthesized JUC-1000 scratched from the carbon cloth. Sharp peaks at 6.32°, 10.96° and 13.44° can perfectly match with (011), (100) and (220) planes for theoretical XRD simulation of JUC-1000 (CCDC-1422688), indicating the successful synthesis of a highly crystalline JUC-1000. The X-ray photoelectron spectroscopy (XPS) survey spectrum confirms the presence of Cu, C, N and O elements for JUC-1000 sample (Fig. S2, ESI). In the Cu 2p region (Fig. 2b), the two binding energies at 934.6 and 953 eV corresponding to Cu $2p_{3/2}$ and Cu $2p_{1/2}$, respectively, and the two at 941 and 962.2 eV attributing to their shake-up satellites (identified as "Sat.") suggest the Cu in the JUC-1000 is in +2 oxidation state. The scanning electron microscopy (SEM) images of JUC-1000/CC (Fig. 2c, d, f and S3, ESI) show that the as-synthesized JUC-1000 is composed of interlaced nanorods with about 1 μm in length and 50 nm in width. The sizes are consistent with the TEM observation (Fig. 2e). Elemental mappings from energy-dispersive X-ray spectroscopy (EDS) reveal uniform distribution of the elements Cu, N and O in the as-prepared JUC-1000/CC (Fig. 2g-i). Obviously, the nanorods are integrated with neighboring ones into hierarchical pores. Such structure ensures the adequate exposure of active sites, and allows electrolyte to easily access inside the pores and pass out, which is very beneficial to enhance mass transfer and catalytic activity.

NRR test was firstly performed under ambient conditions utilizing a H-type electrolytic cell, where two-compartment was separated by a piece of Nafion 115 membrane. JUC-1000/CC as the working electrode was placed in N_2-saturated 1.0 M Na_2SO_4 at the cathode together with a reference electrode, while the counter electrode was placed on the anode. All potentials were iR-compensated and converted to the reversible hydrogen electrode (RHE) scale via calibration. N_2 gas was introduced at a constant flow rate of 10 mL min^{-1} for the entire NRR process for 2 h. The produced NH_3 and N_2H_4 were calculated by calibration curves established by the indophenol blue method[15] and Watt and Chrisp[16] spectrophotometric method.[17] Fig. 3b shows the NH_3 yields and corresponding FEs from the UV-Vis absorption spectra (Fig. 3a) under different potentials ranging from -0.7 V to 0.3 V (vs.RHE). The NH_3 generation rate and FE increase with increasing applied voltage, and reach the highest value of 6.637 mg h^{-1} mg_{cat}^{-1} and 1.519 % at -0.3 V, which is almost an order of magnitude higher than that of bare CC (0.548 mg h^{-1} mg_{cat}^{-1} and 0.19 %) (Fig. S4, ESI). Further increasing the negative voltage decrease the yield rate of NH_3 and FE significantly, which may be attributed to more protons occupy the active sites to accelerate HER. From the corresponding detection calibration curves shown in Fig. S5, ESI, we are pleased to find that the JUC-1000/CC exhibit superduper selectivity toward NRR because no N_2H_4 was detected (Fig. S6, ESI).

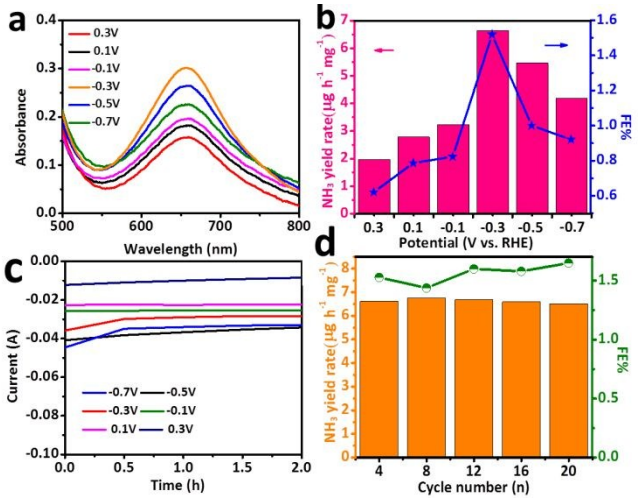

Fig. 3 (a) UV-Vis absorption spectra at different potentials after potentiostatic tests using JUC-1000/CC catalyst in 1.0 M Na_2SO_4. (b) Comparison of NH_3 yields and FEs after potentiostatic tests using JUC-1000/CC catalyst at each given potential. (c) Chronoamperometric curves of JUC-1000/CC in N_2-saturated 1.0 M Na_2SO_4 solution at various potentials. (d) Recycling test results of JUC-1000/CC at -0.3 V.

To further investigate the origin of the excellent activity for JUC-1000/CC, we compared the XPS spectra in the Cu 2p region for the JUC-1000 before and after 20 recycling tests (Fig. S7, ESI). The satellite peak at 941.5 eV disappears, while the new weak peaks at 931.7 and 933.3 eV corresponded to Cu $2p_{3/2}$ are observed, indicating a fraction of electro-reduction for Cu^{II} to Cu^{I} at -0.3 V (vs. RHE) during NRR.[18,19] Therefore, the superior NRR performance of JUC-1000/CC is closely correlated to both Cu^{II}-MOF and Cu^{I}-MOF species. Furtherly, the chronoamperometric tests (Fig. 3c) and consecutive recycling tests (Fig. 3d) were performed. JUC-1000/CC has

neither noticeable fluctuation in the current intensities at several cathodic potentials, nor conspicuously decline of NH_3 yield as well as FE after 20 recycling tests, implying predominant catalytic stability of JUC-1000/CC. The SE-SEM images (Fig. S8, ESI) demonstrates that this catalyst still retains nanorod morphology on CC, while XRD analysis (Fig. S9, ESI) confirm its JUC-1000 nature after the NRR tests despite slightly displacements of diffraction peaks at 6.2°, 18.5°, 22.6° and 36.1°. The strong stability comes from the acidic (-OH) and basic (-NH-, 1, 3, 5-triazine) groups in L ligand of JUC-1000 as the weak acid-base buffer pairs, which is capable of improving the tolerance for Cu paddlewheel MOFs toward water even acidic/alkaline media.[14]

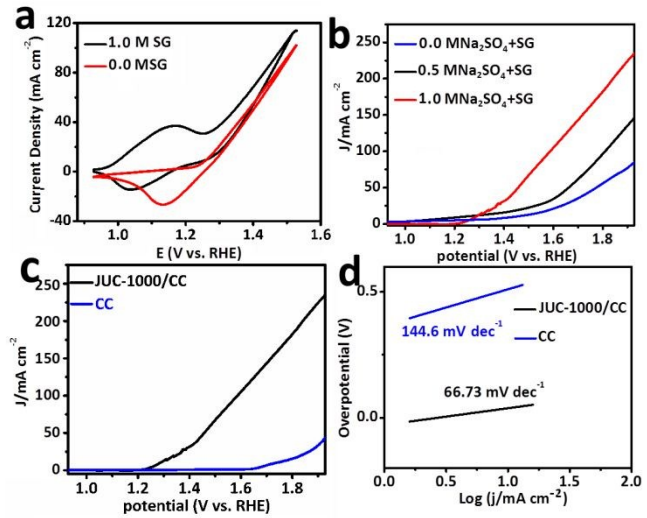

Fig. 4 (a) CV curves of JUC-1000/CC in Na_2SO_4 solution with and without SG. (b) LSV plots of JUC-1000/CC in different concentrations of Na_2SO_4 with 1.0 M SG. (c) LSV plots and (d) Tafel plots for JUC-1000/CC and bare CC in 1.0 M Na_2SO_4 with 1.0 M SG..

To evaluate the feasibility of ECSG replacement of water oxidation, the cyclic voltammetry (CV) test using JUC-1000/CC as the working electrode was conducted in 1.0 M Na_2SO_4 electrolyte with and without 1.0 M SG. As shown in Fig. 4a, a distinct oxidation peak arise at 1.17 V with the introduction of 1.0 M SG, indicating the presence of the ECSG. In contrast, no peak appear in the CV curve without SG, instead of vigorous O_2 evolution is observed. These results suggest that ECSG is thermodynamically more favorable than water oxidation on the JUC-1000/CC. The effect of Na_2SO_4 concentrations on LSV curves was also investigated. Fig. 4b shows that the ECSG activity is improved with Na_2SO_4 solution from 0.0 to 1.0 M, and a further increase of the concentration leads to the decrease of the activity and the produce of precipitation in the electrolyte, indicating the advantage of ECSG in 1.0 M Na_2SO_4. The linear sweep voltammetry (LSV) curves in Fig. 4c indicates that JUC-1000/CC only needs a lower overpotential of 201 mV to achieve 40 mA cm^{-2} current density compare with bare CC (689 mV). Obviously, bare CC has poor ECSG activity without introducing JUC-1000. Fig. 4d. reveals that the Tafel plot for JUC-1000/CC attains 66.73 mV dec^{-1}, outperforming 144.6 mV dec^{-1} of bare CC, implying the favorable catalytic kinetics of JUC-1000/CC for ECSG. From these, we can conclude that the ECSG could efficiently replace OER for decreasing the overpotential of water oxidation.

To evaluate the intrinsic catalytic activity, electrochemical active surface area (ECSA) was acquired by extracting the double layer capacitance (C_{dl}) at the solid/liquid interface.[20] Fig. S10a, b present typical CV curves of JUC-1000/CC and bare CC collected in the region of 0.16 to 0.26 V with scan rates from 70 to 110 mV s^{-1} . The C_{dl} values for JUC-1000/CC and bare CC are estimated to be 10.3 mF cm^{-2} (Fig. 10c) and 9.47 mF cm^{-2} (Fig. S10d) according to the equation $i_c = v \times C_{dl}$,[21] indicating that JUC-1000/CC has a larger electrochemical active surface area and thus more exposed active sites.[22,23] The excellent electrocatalytic activity of JUC-1000/CC was also confirmed by electrochemical impedance spectroscopy (EIS) analysis. Fig. S11 shows that JUC-1000/CC has a smaller radius of a semicircle in comparison with bare CC in 1.0 M Na_2SO_4 solution with SG. Specifically, the charge-transfer resistance (Rct) of JUC-1000/CC (～62.5 ohm) is lower than that for bare CC (～200 ohm), demonstrating a better charge transport capability due to a much lesser charge transfer resistance and more rapid catalytic kinetics.[24,25]

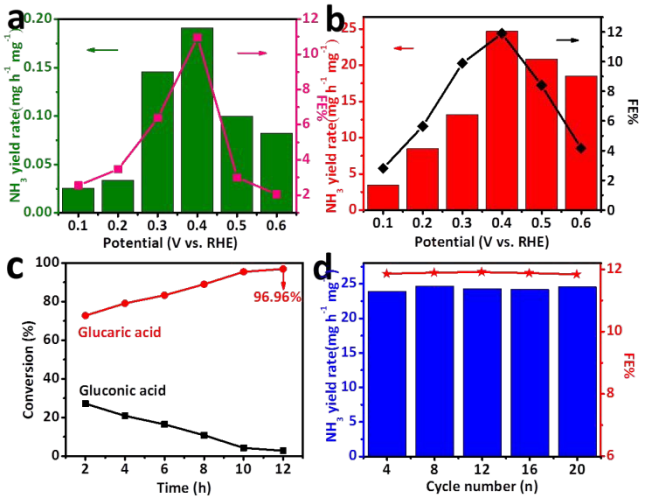

Fig. 5 Electroreduction of N_2 to NH_3 for JUC-1000/CC||JUC-1000/CC in 1.0 M Na_2SO_4 with and without SG. (a) NH_3 yield rates and FEs at different potentials without SG and (b) with SG. (c) Conversion (%) of SG and selectivity (%) of GA at a cell voltage of 0.4 V in 1.0 M Na_2SO_4 with SG. (d) Stability test results for JUC-1000/CC at 0.4 V in 1.0 M Na_2SO_4 with 1.0 M SG under JUC-1000/CC||JUC-1000/CC electrolytic cell device.

We next constructed an H-type electrolytic cell device with two-electrode system, in which JUC-1000/CC were coupled into both anode and cathode (JUC-1000/CC||JUC-1000/CC) for ECSG and NRR simultaneously in Na_2SO_4 electrolyte. NH_3 yields and corresponding FEs with and without SG under different anode voltages were plotted in Fig. 5a and b. The JUC-1000/CC||JUC-1000/CC couple applies a cell voltage of 0.4 V with 1.0 M SG to attain the highest NH_3 yield rate of 24.7 mg h^{-1} mg$_{cat}^{-1}$ and FE% of 11.90, which is higher than the reported some catalysts, such as Ru of 1.3×10^{-3} mg h^{-1} mg$_{cat}^{-1}$ at -1.02 V versus Ag/AgCl, 0.92% at -0.96 V vs. Ag/AgCl and B_4C/CPE of 14.70 μg h^{-1} mg$^{-1}_{cat}$ with an FE of 9.24% at the potential of -0.75 V.[26,27] JUC-1000/CC||RuO_2/CC was also assembled for

compare. As shown in Fig. S12, the NH_3 generation rate for JUC-1000/CC||RuO_2/CC at 0.4 V with 1.0 M SG shows the similar growth as JUC-1000/CC||JUC-1000/CC. However, JUC-1000/CC||JUC-1000/CC behaves a higher NH_3 yield rate of 24.7 mg h^{-1} mg_{cat}^{-1} compared with JUC-1000/CC||RuO_2/CC (20.3 mg h^{-1} mg_{cat}^{-1}).

To explore the role of ECSG in NRR, the comparison test was performed in the anodic electrolyte without SG. Compared with the NRR results upon the addition of 1.0 M SG, it shows a similar level in the FE values (Fig. 5a). Nevertheless, the NH_3 generation rate dramatically decreases over hundredfold with the same potential. Fig. S12, ESI reveals that the HER polarization curve exhibits the potential of -0.74 V vs. RHE to achieve 10 mA cm^{-2} in the presence of SG, which is a negative shift of 10 mV compared with that without SG. The results offer an exciting solution of boosting NRR that the anodic replacement of the water oxidation significantly improves the NH_3 yield and simultaneously maintains FE value accompanied with strong H_2 evolution. This is owing to the more easier oxidition of SG than pure water, such a hybrid electrolyzer can deliver higher current density to the cathode for overall reactions including NH_3 and H_2 generation with lower cell voltage input at the anode, hence increasing the conversion efficiency of the reduction reactions. This conclusion accords with above experimental observations (Fig.5a, b). H_2 evolution is a competitive reaction, but the NH_3 FE value was not decrease with the increase of H_2 yield, indicating that there is no significant selection for the anodic replacement of ECSG.

Fig. 5c displays that the selective oxidations of SG to GA over JUC-1000/CC||JUC-1000/CC at 0.4 V increases with the decreasing concentration of SG during the reaction process. The GA selectivity can reach the high value of 96.96% for 12 h reaction with the SG conversion of 100%, suggesting little side-products in the anode compartment. Impressively, the NH3 yield and FE do not change significantly after 20 cycles tested, implying excellent durability and stability of this JUC-1000/CC catalyst (Fig. 5d).

In summary, we have demonstrated an ECSG strategy for promoting ambient electroreduction of N_2 to NH_3. The assembled electrolyzer utilizing the catalyst, Cu^{II}-MOF/CC as both cathode and anode, needs a cell potential of only 0.4 V to achieve the highest NH_3 yield rate of 24.7mg h^{-1} mg_{cat}^{-1}, FE of 11.90% and GA selectivity of 96.96% in 1.0 M Na_2SO_4 containing 1.0 M SG. Moreover, the NH_3 yield is over hundredfold enhancement and without sacrificing FE value than that of the absence of SG. This study could be further extended for development of other anodic replacement oxidation reaction for energy-efficient NH_3 generation.

Acknowledgements

This work was financially supported by the National Key Scientific Instrument, the Equipment Development Project of China (No. 21627809), the National Natural Science Foundation of China (21605058, 21575050 and 21375047) and the China Postdoctoral Science Foundation (2016M600517).

Conflicts of interest

View Article Online
DOI: 10.1039/C9CC04378K

There are no conflicts to declare.

Notes and references

1 V. Rosc, M. Duca, M. T. de Groot and M. T. Koper, *Chem. Rev.*, 2009, **109**, 2209–2244.
2 G. Chen, X. Cao, S. Wu, X. Zeng, L. Ding, M. Zhu and H. Wang, *J. Am. Chem. Soc.*, 2017, **139**, 9771–9774.
3 M. Ali, F. Zhou, K. Chen, C. Kotzur, C. Xiao, L. Bourgeois, X. Zhang, D. R. MacFarlane, *Nat. Commun*., 2016, **7**, 11335-11339.
4 J. Wang, L. Yu, L. Hu, G. Chen, H. Xin and X. Feng, *Nat. Commun*., 2018, **9**, 1795-1801.
5 V. Kyriakou, I. Garagounis, E. Vasileiou, A. Vourros and M. Stoukides, *Catal. Today*, 2017, **286**, 2–13.
6 X. Guo, H. Du, F. Qu and J. Li, *J. Mater. Chem. A*, 2019, **7**, 3531-3543.
7 B. L. Sheets and G. G. Botte, *Chem. Commun.*, 2018, **54**, 4250-4253.
8 K. Kim, N. Lee, C. Y. Yoo, J. N. Kim, H. C. Yoon and J. I. Han, *J. Electrochem. Soc.*, 2016, **163**, F610–F612.
9 F. Zhou, L. M. Azofra, M. Ali, M. Kar, A. N. Simonov, C. McDonnell-Worth, C. Sun, X. Zhang and D. R. MacFarlane, *Energy Environ. Sci.*, 2017, **10**, 2516.
10 Z. Zhang and G. W. Huber, *Chem. Soc. Rev.*, 2018, **47**, 1351-1390.
11 J. Lee, B. Saha and D. G. Vlachos, *Green Chem.*, 2016, **18**, 3815-3822.
12 S. V. de Vyver and Y. Roma ´n-Leshkov, *Catal. Sci. Technol.*,2013, **3**, 1465–1479.
13 S. Zheng, X. Li, B. Yan, Q. Hu, Y. Xu, X. Xiao, H. Xue and H. Pang, *Adv. Energy Mater.*, 2017, **7**, 2733-2755.
14 H. He, Q. Sun, W. Gao, J. A. Perman, F. Sun, G. Zhu, B. Aguila, K. Forrest, B. Space and S. Ma, *Angew. Chem. Int. Ed.*, 2018, **130**, 4747-4752.
15 D. H. He, J. J. Liu, Y. Wang, F. Li, B. Li and J. B. He. *Electrochimica Acta., 2*019, **308**, 285-294.
16 H. Chen, Y. Gao, L. Ye, Y. N. Yao, X. Y. Chen, Y. Wei and L. C. Sun. *Chem. Commun.*, 2018, **54**, 4979-4982.
17 D. Zhu, L. Zhang, R. E. Ruther and R. J. Hamers, *Nat. Mater.*, 2013, **12**, 836–841.
18 G. W. Watt andJ. D. Chrisp, *Anal. Chem.*, 1952, **24**, 2006–2008.
19 C. Li, T. Wang, Z. Zhao, W. Yang, J. Li, A. Li, Z. Yang, G. A. Ozin, and J. Gong, *Angew. Chem. Int. Ed.*, 2018, **130**, 5376-5380.
20 S. Trasatti and O. A. Petrii, *J. Electroanal. Chem.*, 1992, **327**, 353–376.
21 C. C. L. McCrory, J. C. Peters and T. F. Jaramillo, *J. Am. Chem. Soc.*, 2013, **135**, 16977−16987.
22 X. Ren, X. Ji, Y. Wei, D. Wu, Y. Zhang, M. Ma, Z. Liu, Abdullah M. Asiri, Q. Wei and X. Sun, *Chem. Commun.*, 2018, **54**, 1425-1428.
23 D. Wu, Y. Wei, X. Ren, X. Ji, Y. Liu, X. Guo, Z. Liu, A. M. Asiri, Q. Wei and X. Sun, *Adv. Mater.*, 2018, **30**, 5366-5372.
24 M. J. Kang, H. Parkb, J. Jegal, S. Y. Hwang,Y. S. Kanga and H. G. Cha, *Appl Catal B-Environ.*, 2019, **242**, 85–91.
25 X. Ren, D. Wu, R. Ge, X. Sun, H. Ma. T. Yan, Y. Zhang, B. Du, Q. Wei and L. Chen, *Nano Res.*, 2018, **11**, 2024-2033.
26 V. Kordali, G. Kyriacou and C. Lambrou, *Chem. Commun.*, 2000, **17**, 1673–1674.
27 W. Qiu, X. Xie, J. Qiu, W. Fang, R. Liang, X. Ren, X. Ji, G. Cui, A. M. Asiri, G. Cui, B Tang and X. Sun, *Nat. Commun*. 2018, **9**, 3485-3492.